M&C 2017 - International Conference on Mathematics & Computational Methods Applied to Nuclear Science & Engineering, Jeju, Korea, April 16-20, 2017, on USB (2017)

Acceleration of Step and Linear Discontinuous Schemes for the Method of Characteristics in DRAGON5

Alain Hébert

École Polytechnique de Montréal
C.P. 6079 succ. "Centre-Ville", Montréal Qc. CANADA H3C 3A7
alain.hebert@polymtl.ca

Abstract - *We are investigating the applicability of the algebraic collapsing acceleration (ACA) technique to the method of characteristics (MOC) in cases with scattering anisotropy and/or linear sources. Previously, the ACA was proven successful in cases with isotropic scattering and uniform (step) sources. A presentation is first made of the MOC implementation, available in the DRAGON5 code. Two categories of schemes are available for integrating the propagation equations: the first category is based on exact integration and leads to the classical step characteristics (SC) and linear discontinuous characteristics (LDC) schemes. The second category leads to diamond differencing schemes of various orders in space. We focus on the acceleration of these MOC schemes using a combination of the generalized minimal residual (GMRES(m)) method preconditioned with the ACA technique. Numerical results are provided for a 2D eight-symmetry PWR assembly mockup in the context of the DRAGON5 code.*

I. INTRODUCTION

This paper is related to the application of the method of characteristics (MOC) for solving the neutron transport equation.[1] We are investigating a new class of linear characteristics schemes along cyclic tracks for solving the transport equation for neutral particles with scattering anisotropy. These algorithms rely on step and linear discontinuous exact integration, as described in Refs. [2] and [3]. These schemes are based on linear discontinuous coefficients that are derived through the application of approximations describing the mesh-averaged spatial flux moments in terms of spatial source moments and of the beginning- and end-of-segment flux values. The *linear discontinuous characteristics* (LDC) scheme is inherently conservative, a property that facilitate its practical implementation and the acceleration of its scattering iterations in a production code such as DRAGON5.[4] In this paper, we focus on the acceleration of the scattering iterations who are required with the application of the MOC. Two acceleration techniques are investigated: the *generalized minimal residual* (GMRES(m)) method[5] and the *algebraic collapsing acceleration* (ACA) method.[6] The application of these techniques was demonstrated on a 2D eight-symmetry PWR assembly mockup in the context of the DRAGON5 code. It is shown that the acceleration remains effective in spite of the introduction of scattering anisotropy and linear sources.

II. THEORY

We give a brief introduction of the MOC formalism. The boundary conditions treatment along with the details on the iterative strategy are not reported in the present paper but can be found in Ref. [1]. The classical SC and DD0 schemes are also presented in this book. Emphasis is put on the characteristic form of the transport equation which arises from the trajectory-based formulation of the flux integration. The conservation principle is formulated within this framework.

The backward *characteristic form of the transport equation* was obtained in Sect. 3.2.1 of Ref. [1]. The one-speed and steady-state form of this equation is written

$$\frac{d}{ds}\phi(\boldsymbol{r}+s\,\boldsymbol{\Omega},\boldsymbol{\Omega})+\Sigma(\boldsymbol{r}+s\,\boldsymbol{\Omega})\,\phi(\boldsymbol{r}+s\,\boldsymbol{\Omega},\boldsymbol{\Omega}) = Q(\boldsymbol{r}+s\,\boldsymbol{\Omega},\boldsymbol{\Omega}) \quad (1)$$

where $\boldsymbol{r}$ is the starting point of the particle, s is the distance travelled by the particle on its characteristic, $\boldsymbol{\Omega}$ is the direction of the characteristic, $\Sigma(\boldsymbol{r})$ is the value of the macroscopic total cross section at $\boldsymbol{r}$, $\phi(\boldsymbol{r},\boldsymbol{\Omega})$ is the particle angular flux at $\boldsymbol{r}$, and $Q(\boldsymbol{r},\boldsymbol{\Omega})$ is the fixed source at $\boldsymbol{r}$.

The spatial integration domain is partitioned into regions of volume $\{V_i\,;\ i=1,I\}$, each of them characterized by uniform nuclear properties and surrounded by boundary surfaces $\{S_\alpha\,;\ \alpha=1,\Lambda\}$. The MOC is based on the discretization of Eq. (1) along each path of the particle and on the integration of the flux contributions using spatial integrals of the form

$$\begin{aligned} V_i\phi_i &= \int_{V_i} d^3r \int_{4\pi} d^2\Omega\,\phi(\boldsymbol{r},\boldsymbol{\Omega}) \\ &= \int_{\Upsilon} d^4T \int_{-\infty}^{\infty} ds\,\chi_{V_i}(\boldsymbol{T},s)\,\phi(\boldsymbol{p}+s\boldsymbol{\Omega},\boldsymbol{\Omega}) \end{aligned} \quad (2)$$

where ϕ_i is the average flux in region i and $\Upsilon=\{\boldsymbol{T}\}$ is the tracking domain. A single characteristic $\boldsymbol{T}$ is determined by its orientation $\boldsymbol{\Omega}$ and its starting point $\boldsymbol{p}$ defined on a reference plane $\boldsymbol{\Pi_\Omega}$ perpendicular to $\boldsymbol{T}$, as depicted in Fig. 1. The characteristics are selected in domain $\Upsilon=4\pi\times\boldsymbol{\Pi_\Omega}$ which is characterized by an order-four differential $d^4T=d^2\Omega\,d^2p$. The local coordinate s defines the distance of point $\boldsymbol{r}$ with respect to plane $\boldsymbol{\Pi_\Omega}$. Finally, the characteristic function $\chi_{V_i}(\boldsymbol{T},s)$ is equal to one if point $\boldsymbol{p}+s\boldsymbol{\Omega}$ of characteristic $\boldsymbol{T}$ is located inside V_i, and zero otherwise.

The MOC requires knowledge of region indices N_k and segment lengths ℓ_k describing the overlapping of characteristic $\boldsymbol{T}$ with the domain. This information is written $\{N_k,\ell_k\,;\ k=1,K\}$ where K is the total number of regions crossed by $\boldsymbol{T}$. It is important to note that segment lengths ℓ_k are *always* defined in 3D, even for prismatic 2–D geometries. The intersection points of a characteristic with the region boundaries, and the corresponding angular flux on these

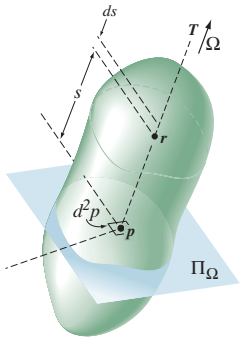

Fig. 1. Spatial integration domain.

boundaries, are written

$$\boldsymbol{r}_{k+1} = \boldsymbol{r}_k + \ell_k\,\boldsymbol{\Omega};\;\; k = 1, K. \tag{3}$$

1. The linear discontinuous characteristic assumption in space

We introduce a linear representation of the sources along characteristic $\boldsymbol{T}$ based on an expansion in normalized Legendre polynomials. This expansion is applied over segment $\ell_k(\boldsymbol{T})$, as pictured in Fig. 2. Its mathematical expression is

$$Q(\boldsymbol{r}_k + s\,\boldsymbol{\Omega}, \boldsymbol{\Omega}) = Q_k^{(0)}(\boldsymbol{\Omega}) + 2\sqrt{3}\left[s - \frac{\ell_k(\boldsymbol{T})}{2}\right] Q_k^{(1)}(\boldsymbol{\Omega});\;\; k = 1, K \tag{4}$$

where

$$Q_k^{(0)}(\boldsymbol{\Omega}) = \frac{1}{\ell_k(\boldsymbol{T})}\int_0^{\ell_k(\boldsymbol{T})} ds\, Q(\boldsymbol{r}_k + s\,\boldsymbol{\Omega}, \boldsymbol{\Omega}) \tag{5}$$

and

$$Q_k^{(1)}(\boldsymbol{\Omega}) = \frac{2\sqrt{3}}{\ell_k^3(\boldsymbol{T})}\int_0^{\ell_k(\boldsymbol{T})} ds\left[s - \frac{\ell_k(\boldsymbol{T})}{2}\right] Q(\boldsymbol{r}_k + s\,\boldsymbol{\Omega}, \boldsymbol{\Omega}). \tag{6}$$

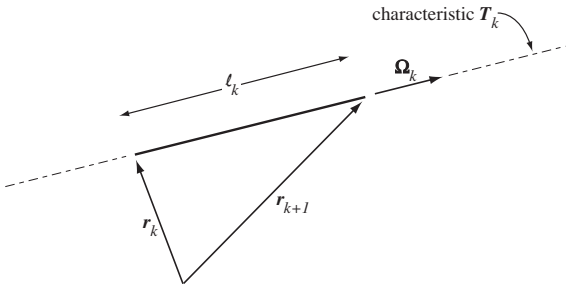

Fig. 2. A segment of a single characteristic.

Knowledge of the moments of the flux over segment $\ell_k(\boldsymbol{T})$ are required in order to compute components of the source, $Q_k^{(0)}(\boldsymbol{\Omega})$ and $Q_k^{(1)}(\boldsymbol{\Omega})$. The moments of the segment-averaged fluxes are defined as

$$\bar{\phi}_k^{(0)}(\boldsymbol{T}) = \frac{1}{\ell_k(\boldsymbol{T})}\int_0^{\ell_k(\boldsymbol{T})} ds\,\phi(\boldsymbol{r}_k + s\,\boldsymbol{\Omega}, \boldsymbol{\Omega}) \tag{7}$$

and

$$\bar{\phi}_k^{(1)}(\boldsymbol{T}) = \frac{2\sqrt{3}}{\ell_k^3(\boldsymbol{T})}\int_0^{\ell_k(\boldsymbol{T})} ds\left[s - \frac{\ell_k(\boldsymbol{T})}{2}\right]\phi(\boldsymbol{r}_k + s\,\boldsymbol{\Omega}, \boldsymbol{\Omega}). \tag{8}$$

Substitution of the linear source approximation (4) into the characteristics form of the transport equation leads to

$$\begin{aligned}\frac{d}{ds}\phi(\boldsymbol{r}_k + s\,\boldsymbol{\Omega}, \boldsymbol{\Omega}) + \Sigma_{N_k}\phi(\boldsymbol{r}_k + s\,\boldsymbol{\Omega}, \boldsymbol{\Omega}) \\ = Q_k^{(0)}(\boldsymbol{\Omega}) + 2\sqrt{3}\left[s - \frac{\ell_k(\boldsymbol{T})}{2}\right] Q_k^{(1)}(\boldsymbol{\Omega}).\end{aligned} \tag{9}$$

Analytical solution of equation (9) is written

$$\begin{aligned}\phi(\boldsymbol{r}_k + s\,\boldsymbol{\Omega}, \boldsymbol{\Omega}) &= \phi(\boldsymbol{r}_k, \boldsymbol{\Omega})\,\mathrm{e}^{-s\,\Sigma_{N_k}} + \frac{Q_k^{(0)}(\boldsymbol{\Omega})}{\Sigma_{N_k}}\left(1 - \mathrm{e}^{-s\,\Sigma_{N_k}}\right) \\ &+ \frac{\sqrt{3}\,Q_k^{(1)}(\boldsymbol{\Omega})}{\Sigma_{N_k}^2}\left[2\mathrm{e}^{-s\,\Sigma_{N_k}} + 2\,(s\,\Sigma_{N_k} - 1)\right. \\ &- \left.\Sigma_{N_k}\ell_k(\boldsymbol{T})\left(1 - \mathrm{e}^{-s\,\Sigma_{N_k}}\right)\right].\end{aligned} \tag{10}$$

where $\phi_k(\boldsymbol{T}) = \phi(\boldsymbol{r}_k, \boldsymbol{\Omega})$.

Setting $\phi_k(\boldsymbol{T}) \equiv \phi(\boldsymbol{r}_k, \boldsymbol{\Omega})$ and $\phi_{k+1}(\boldsymbol{T}) \equiv \phi(\boldsymbol{r}_k + \ell_k(\boldsymbol{T})\,\boldsymbol{\Omega}, \boldsymbol{\Omega})$, it is possible to write the propagation equations for the MOC with linear source approximation and anisotropic scattering as

$$\begin{aligned}\phi_{k+1}(\boldsymbol{T}) &= \mathcal{A}_k(\boldsymbol{T})\,\phi_k(\boldsymbol{T}) + \mathcal{B}_k(\boldsymbol{T})\,Q_k^{(0)}(\boldsymbol{\Omega}) \\ &+ C_k(\boldsymbol{T})\,\ell_k(\boldsymbol{T})\,Q_k^{(1)}(\boldsymbol{\Omega}) \\ \bar{\phi}_k^{(0)}(\boldsymbol{T}) &= \frac{1}{\ell_k(\boldsymbol{T})}\Big[\mathcal{B}_k(\boldsymbol{T})\,\phi_k(\boldsymbol{T}) + \mathcal{D}_k(\boldsymbol{T})\,Q_k^{(0)}(\boldsymbol{\Omega}) \\ &+ \mathcal{E}_k(\boldsymbol{T})\,\ell_k(\boldsymbol{T})\,Q_k^{(1)}(\boldsymbol{\Omega})\Big] \\ \bar{\phi}_k^{(1)}(\boldsymbol{T}) &= \frac{1}{\ell_k(\boldsymbol{T})^2}\Big[\mathcal{F}_k(\boldsymbol{T})\,\phi_k(\boldsymbol{T}) + \mathcal{G}_k(\boldsymbol{T})\,Q_k^{(0)}(\boldsymbol{\Omega}) \\ &+ \mathcal{H}_k(\boldsymbol{T})\,\ell_k(\boldsymbol{T})\,Q_k^{(1)}(\boldsymbol{\Omega})\Big]\end{aligned} \tag{11}$$

where the set of coefficients $\mathcal{A}_k(\boldsymbol{T})$ to $\mathcal{H}_k(\boldsymbol{T})$ can take different values, depending on the type of MOC approximation and on the magnitude of the optical path $\tau_k(\boldsymbol{T})$. The set of coefficient corresponding to the LDC case with $\tau_k(\boldsymbol{T}) \geq \epsilon$ is

$$\begin{aligned}\mathcal{A}_k(\boldsymbol{T}) &= \mathrm{e}^{-\tau_k(\boldsymbol{T})} \qquad \mathcal{B}_k(\boldsymbol{T}) = \frac{1}{\Sigma_{N_k}}\left(1 - \mathrm{e}^{-\tau_k(\boldsymbol{T})}\right) \\ C_k(\boldsymbol{T}) &= \frac{\sqrt{3}}{\tau_k(\boldsymbol{T})\,\Sigma_{N_k}}\left(2\mathrm{e}^{-\tau_k(\boldsymbol{T})} + \tau_k(\boldsymbol{T}) - 2 + \tau_k(\boldsymbol{T})\,\mathrm{e}^{-\tau_k(\boldsymbol{T})}\right) \\ \mathcal{D}_k(\boldsymbol{T}) &= \frac{\ell_k(\boldsymbol{T})}{\Sigma_{N_k}}\left(1 - \frac{1 - \mathrm{e}^{-\tau_k(\boldsymbol{T})}}{\tau_k(\boldsymbol{T})}\right) \\ \mathcal{E}_k(\boldsymbol{T}) &= -\frac{\sqrt{3}}{\tau_k(\boldsymbol{T})\,\Sigma_{N_k}^2}\left(2\mathrm{e}^{-\tau_k(\boldsymbol{T})} + \tau_k(\boldsymbol{T}) - 2 + \tau_k(\boldsymbol{T})\,\mathrm{e}^{-\tau_k(\boldsymbol{T})}\right) \\ \mathcal{F}_k(\boldsymbol{T}) &= -\frac{\sqrt{3}}{\tau_k(\boldsymbol{T})\Sigma_{N_k}}\left(2\mathrm{e}^{-\tau_k(\boldsymbol{T})} + \tau_k(\boldsymbol{T}) - 2 + \tau_k(\boldsymbol{T})\,\mathrm{e}^{-\tau_k(\boldsymbol{T})}\right) \\ \mathcal{G}_k(\boldsymbol{T}) &= \frac{\sqrt{3}}{\tau_k(\boldsymbol{T})\Sigma_{N_k}^2}\left(2\mathrm{e}^{-\tau_k(\boldsymbol{T})} + \tau_k(\boldsymbol{T}) - 2 + \tau_k(\boldsymbol{T})\,\mathrm{e}^{-\tau_k(\boldsymbol{T})}\right) \\ \mathcal{H}_k(\boldsymbol{T}) &= \frac{1}{\tau_k(\boldsymbol{T})^2\,\Sigma_{N_k}^2}\Big(12 - 12\,\mathrm{e}^{-\tau_k(\boldsymbol{T})} - 3\,\tau_k(\boldsymbol{T})^2 + \tau_k(\boldsymbol{T})^3 \\ &- 3\,\tau_k(\boldsymbol{T})^2\,\mathrm{e}^{-\tau_k(\boldsymbol{T})} - 12\,\tau_k(\boldsymbol{T})\,\mathrm{e}^{-\tau_k(\boldsymbol{T})}\Big).\end{aligned} \tag{12}$$

Otherwise, in case of small optical path, Taylor expansions of the above relations are used.

Solution of Eqs. (12) over a finite track is straightforward. Each track is travelled back and forth starting from the initial boundary where $\phi_1(\boldsymbol{T})$ or $\phi_{K+1}(-\boldsymbol{T})$ is set. This approach is simpler than the algorithm proposed in Ref. [2], but leads to the same solution.

Solution of Eqs. (12) over a cyclic track is based on the requirement that $\phi_{K+1}(\boldsymbol{T}) = \phi_1(\boldsymbol{T})$ where K is the total number of segments in all the subtracks constituting the track $\boldsymbol{T}$. A recursion is applied, as described in Ref. [3].

2. Determination of the spherical harmonics coefficients

Expressions of the segment-averaged fluxes $\bar{\phi}_k^{(0)}(\boldsymbol{T}_n)$ and $\bar{\phi}_k^{(1)}(\boldsymbol{T}_n)$ are expanded in spherical harmonics. The uniform component of the flux in direction $\boldsymbol{\Omega}_n$ for the track $\boldsymbol{T}_n$ is defined as

$$\bar{\phi}_k^{(0)}(\boldsymbol{T}_n) = \sum_{\ell=0}^{\infty} \frac{2\ell+1}{4\pi} \sum_{\substack{m=-\ell \\ \ell+m \text{ even}}}^{\ell} \bar{\phi}_{\ell,k}^m R_\ell^m(\boldsymbol{\Omega}_n) \tag{13}$$

and the linear component of the flux in direction $\boldsymbol{\Omega}_n$ for the track $\boldsymbol{T}_n$ is defined from its Cartesian components as

$$\bar{\phi}_k^{(1)}(\boldsymbol{T}_n) = \sum_{\ell=0}^{\infty} \frac{2\ell+1}{4\pi} \sum_{\substack{m=-\ell \\ \ell+m \text{ even}}}^{\ell} \left[\boldsymbol{\nabla}\bar{\phi}_{\ell,k}^m \cdot \boldsymbol{\Omega}\right] R_\ell^m(\boldsymbol{\Omega}_n). \tag{14}$$

Here, important remarks should be made concerning Eqs. (13) and (14). We are *not* assuming limited expansions for $\bar{\phi}_k^{(0)}(\boldsymbol{T}_n)$ and $\bar{\phi}_k^{(1)}(\boldsymbol{T}_n)$. Equations (13) and (14) are introduced as a convenient way to define the flux moments $\bar{\phi}_{\ell,k}^m$ and $\boldsymbol{\nabla}\bar{\phi}_{\ell,k}^m$ that need to be evaluated up to the order of the anisotropic source. Angular accuracy of the flux is limited by the number of discrete angles used in the tracking, not by a limited spherical harmonic expansion. Finally, we assume a 2–D geometry, so that only even $\ell + m$ indices are used and so that flux moments $\boldsymbol{\nabla}\bar{\phi}_{\ell,k}^m$ are two-component vectors. The high-order property of our characteristics scheme in space comes from the introduction of Eq. (14).

Two conditions have to be fulfilled in order for the MOC scheme to be inherently conservative. *(1)* The balance equation must be imposed on each track, and *(2)* Consistent spherical harmonic moments must be defined for $\bar{\phi}_{\ell,k}^m$ and $\boldsymbol{\nabla}\bar{\phi}_{\ell,k}^m$ in Eqs. (13) and (14). This second condition is more difficult to reach for the LDC and DD1 schemes, due to the non-orthogonality of the spherical harmonic basis $\boldsymbol{\Omega} R_\ell^m(\boldsymbol{\Omega})$.

Equation (13) is a plain spherical harmonic expansion. Its segment-averaged coefficients are therefore written

$$\bar{\phi}_{\ell,k}^m = \int_{4\pi} d^2\Omega\, R_\ell^m(\boldsymbol{\Omega})\, \bar{\phi}_k^{(0)}(\boldsymbol{T}_n)\ ; \quad \ell \le L \tag{15}$$

and can be collapsed into region-averaged spherical harmonic moment ϕ_{ℓ,N_k}^m, where N_k is the region index containing segment k.

The determination of coefficients $\boldsymbol{\nabla}\phi_{\ell,N_k}^m \equiv \text{col}(\frac{\partial}{\partial x}\phi_{\ell,N_k}^m, \frac{\partial}{\partial y}\phi_{\ell,N_k}^m)$ is now presented. Unfortunately, the trial functions $\boldsymbol{\Omega} R_\ell^m(\boldsymbol{\Omega})$ are not mutually orthogonal. Off-diagonal contributions need to be taken into account. As presented in Ref. [2], the spherical harmonics coefficients $\boldsymbol{\psi}_{\ell,N_k}^m$ are a linear combination of the slope components $\boldsymbol{\nabla}\phi_{\ell,N_k}^m$. The MOC procedure proceed in two steps:

- We first set the first $L+2$ segment-averaged moments of $\bar{\phi}_k^{(1)}(\boldsymbol{T}_n)$ as two-component vectors written

$$\bar{\boldsymbol{\psi}}_{\ell,k}^m = \int_{4\pi} d^2\Omega\, \boldsymbol{\Omega}\, R_\ell^m(\boldsymbol{\Omega})\, \bar{\phi}_k^{(1)}(\boldsymbol{T}_n). \tag{16}$$

  We compute the region-averaged moments $\boldsymbol{\psi}_{\ell,N_k}^m$ by collapsing these segment-averaged moments $\bar{\boldsymbol{\psi}}_{\ell,k}^m$.

- Compute the slope components $\boldsymbol{\nabla}\phi_{\ell,i}^m$ in each region i by inverting the following relation[2]

$$\boldsymbol{\psi}_{\ell,i}^m = \sum_{\ell'=0}^{L+2} \frac{2\ell'+1}{4\pi} \sum_{\substack{m'=-\ell' \\ \ell'+m' \text{ even}}}^{\ell'} \mathbb{M}_{\ell,\ell'}^{m,m'} \cdot \boldsymbol{\nabla}\phi_{\ell',i}^{m'} \tag{17}$$

  where $\ell \le L+2$ and where the dyadic coefficients are written

$$\mathbb{M}_{\ell,\ell'}^{m,m'} = \int_{4\pi} d^2\Omega\, (\boldsymbol{\Omega} \otimes \boldsymbol{\Omega})\, R_\ell^m(\boldsymbol{\Omega})\, R_{\ell'}^{m'}(\boldsymbol{\Omega}). \tag{18}$$

Only a 2×2 submatrix of $\mathbb{M}_{\ell,\ell'}^{m,m'}$ is worthwhile to analyze 2–D geometries, based on the following definition of

$$\boldsymbol{\Omega} \otimes \boldsymbol{\Omega} = \begin{bmatrix} R_1^1(\boldsymbol{\Omega})R_1^1(\boldsymbol{\Omega}) & R_1^1(\boldsymbol{\Omega})R_1^{-1}(\boldsymbol{\Omega}) \\ R_1^1(\boldsymbol{\Omega})R_1^{-1}(\boldsymbol{\Omega}) & R_1^{-1}(\boldsymbol{\Omega})R_1^{-1}(\boldsymbol{\Omega}) \end{bmatrix}. \tag{19}$$

Calculation of coefficients $\mathbb{M}_{\ell,\ell'}^{m,m'}$ up to order P_3 is presented in Ref. [2]. In the simple case of isotropic scattering sources, moments $\boldsymbol{\psi}_{0,i}^0$ are a linear combination of slope components $\boldsymbol{\nabla}\phi_{0,i}^0$ and $\boldsymbol{\nabla}\phi_{2,i}^m$. After inversion of Eq. (17), calculation of $\boldsymbol{\nabla}\phi_{0,i}^0$ requires knowledge of $\boldsymbol{\psi}_{0,i}^0$ and $\boldsymbol{\psi}_{2,i}^m$. This procedure is required for making the LDC and DD1 schemes inherently conservative.

We should also remember an important issue presented in Ref. [2]. There is an inherent singularity with the linear coefficients of Eq. (17) at each Legendre order with $\ell > 0$. It is therefore not possible to determine the moments of the flux gradient $\boldsymbol{\nabla}\phi_{\ell,i}^m$ by performing a simple inversion of Eq. (17). The approach proposed in Ref. [2] consists to add heuristic equations to the linear system and to perform a pseudo-inversion of the resulting rectangular matrix. We have been able to find heuristic equations up to P_3 order.

Using Eq. (7), it is possible to rewrite Eq. (2) as

$$V_i\phi_i^{(0)} = \int_\Upsilon d^4T \sum_k \delta_{iN_k}\, \ell_k(\boldsymbol{T})\, \bar{\phi}_k^{(0)}(\boldsymbol{T}) \tag{20}$$

where δ_{ij} is the Kronecker delta function and where the summation over k is performed over all the existing indices. All

the characteristics $\boldsymbol{T}$ are spanned in Eq. (20), but only those that effectively cross region i contribute to the integral. We introduce a summation over characteristics with index $n \leq N$, with N as the total number of characteristics. Note that each track of the tracking object is used twice as two characteristics, in $\boldsymbol{\Omega}_n$ and $-\boldsymbol{\Omega}_n$ directions.

Using the same approach that leads to Eq. (20), the volume of region i is written

$$4\pi\, V_i = \int_{\Upsilon} d^4T \sum_k \delta_{iN_k}\, \ell_k(\boldsymbol{T}). \tag{21}$$

Equation (21) is the numerical approximation used in MOC for the numerical volumes. The effect of this approximation can be mitigated by renormalizing tracking in order to force the equality. Two renormalization options are available, depending if the normalization factors are function or not of the track directions.

The next relation is the main approximations behind the proposed MOC. It consists to compute spherical harmonic moments of the flux over segments using Eq. (15) and to smear these contributions over computational regions. This relation is written

$$\frac{1}{4\pi}\phi^m_{\ell,i} = \frac{\sum\limits_{n=1}^{N} \omega_n \sum\limits_k \delta_{iN_k}\, \ell_k(\boldsymbol{T}_n)\, \bar{\phi}^{(0)}_k(\boldsymbol{T}_n)\, R^m_\ell(\boldsymbol{\Omega}_n)}{\sum\limits_{n=1}^{N} \omega_n \sum\limits_k \delta_{iN_k}\, \ell_k(\boldsymbol{T}_n)} \tag{22}$$

where the averaged segment flux $\bar{\phi}^{(0)}_k(\boldsymbol{T}_n)$ can be evaluated from the propagation Eqs. (12).

In the context of the LDC and DD1 schemes, Eq. (22) is still used, in conjunction with Eqs. (12). The basic relation allowing MOC to construct the slope-related moments $\boldsymbol{\psi}^m_{\ell,i}$ is obtained from Eq. (16), using trial functions $R^m_\ell(\boldsymbol{\Omega}_n)\,\boldsymbol{\Omega}_n$, as

$$\frac{1}{4\pi}\boldsymbol{\psi}^m_{\ell,i} = \frac{\sum\limits_{n=1}^{N} \omega_n \sum\limits_k \delta_{iN_k}\, \ell_k(\boldsymbol{T}_n)\, \bar{\phi}^{(1)}_k(\boldsymbol{T}_n)\, R^m_\ell(\boldsymbol{\Omega}_n)\,\boldsymbol{\Omega}_n}{\sum\limits_{n=1}^{N} \omega_n \sum\limits_k \delta_{iN_k}\, \ell_k(\boldsymbol{T}_n)}. \tag{23}$$

An assumption is made on the anisotropy order L of the scattering sources. The uniform source in direction $\boldsymbol{\Omega}_n$ is defined as

$$Q^{(0)}_{N_k}(\boldsymbol{\Omega}_n) = \sum_{\ell=0}^{L} \frac{2\ell+1}{4\pi} \sum_{\substack{m=-\ell \\ \ell+m \text{ even}}}^{\ell} Q^m_{\ell,N_k} R^m_\ell(\boldsymbol{\Omega}_n). \tag{24}$$

The linear source in direction $\boldsymbol{\Omega}_n$ is defined from its Cartesian components as

$$Q^{(1)}_{N_k}(\boldsymbol{\Omega}_n) = \sum_{\ell=0}^{L} \frac{2\ell+1}{4\pi} \sum_{\substack{m=-\ell \\ \ell+m \text{ even}}}^{\ell} \left[\boldsymbol{\nabla} Q^m_{\ell,N_k} \cdot \boldsymbol{\Omega}_n\right] R^m_\ell(\boldsymbol{\Omega}_n). \tag{25}$$

The spherical harmonic moments of the sources are expressed as a function of fixed sources $S^m_{\ell,i}$ and scattering information as

$$Q^m_{\ell,i} = S^m_{\ell,i} + \Sigma_{\mathrm{s},\ell,i}\, \phi^m_{\ell,i} \tag{26}$$

and

$$\boldsymbol{\nabla} Q^m_{\ell,i} = \boldsymbol{\nabla} S^m_{\ell,i} + \Sigma_{\mathrm{s},\ell,i} \boldsymbol{\nabla} \phi^m_{\ell,i}\,. \tag{27}$$

III. SYNTHETIC ACCELERATION

The particle source distribution $Q(\boldsymbol{r}, \boldsymbol{\Omega})$ appearing in the right-hand side of the transport Eq. (1) is written in terms of the within-group scattering reaction rate using

$$Q(\boldsymbol{r}, \boldsymbol{\Omega}) = \sum_{\ell=0}^{L} \frac{2\ell+1}{4\pi} \sum_{m=-\ell}^{\ell} \left[\Sigma_{\mathrm{w},\ell}(\boldsymbol{r})\, \phi^m_\ell(\boldsymbol{r}) + Q^{\diamond m}_\ell(\boldsymbol{r})\right] R^m_\ell(\boldsymbol{\Omega}) \tag{28}$$

where $\Sigma_{\mathrm{w},\ell}(\boldsymbol{r})$ is the ℓ-th Legendre moment of the macroscopic within-group scattering cross section, $\Phi^m_\ell(\boldsymbol{r})$ is a spherical harmonic component of the flux and $Q^{\diamond m}_\ell(\boldsymbol{r})$ is a spherical harmonic component of the source representing other contributions such as fission and out-of-group scattering rates. Scattering source iterations are always required with the MOC. Introducing an iteration index (κ), the basic *scattering source iterative scheme* is written

$$\begin{aligned} &\frac{d}{ds}\phi^{(\kappa+1)}(\boldsymbol{r} + s\,\boldsymbol{\Omega}, \boldsymbol{\Omega}) + \Sigma(\boldsymbol{r} + s\,\boldsymbol{\Omega})\, \phi^{(\kappa+1)}(\boldsymbol{r} + s\,\boldsymbol{\Omega}, \boldsymbol{\Omega}) \\ &\quad = \sum_{\ell=0}^{L} \frac{2\ell+1}{4\pi} \sum_{m=-\ell}^{\ell} \Big[\Sigma_{\mathrm{w},\ell}(\boldsymbol{r} + s\,\boldsymbol{\Omega})\, \phi^{m,(\kappa)}_\ell(\boldsymbol{r} + s\,\boldsymbol{\Omega}) \\ &\quad + Q^{\diamond m}_\ell(\boldsymbol{r} + s\,\boldsymbol{\Omega})\Big] R^m_\ell(\boldsymbol{\Omega}) \end{aligned} \tag{29}$$

where $\Phi^{m,(\kappa)}_\ell(\boldsymbol{r})$ are the spherical harmonic flux component computed with the MOC at the (κ)-th iteration.

As pointed out in Ref. [7], the fixed-point convergence of Eq. (29) becomes difficult with large domains or in the presence of purely scattering media as the scattering ratio approaches one. In this case, Alcouffe proposed a preconditioning known as *synthetic acceleration*, based on the following scheme:

$$\begin{aligned} &\frac{d}{ds}\phi^{(\kappa+\frac{1}{2})}(\boldsymbol{r} + s\,\boldsymbol{\Omega}, \boldsymbol{\Omega}) + \Sigma(\boldsymbol{r} + s\,\boldsymbol{\Omega})\, \phi^{(\kappa+\frac{1}{2})}(\boldsymbol{r} + s\,\boldsymbol{\Omega}, \boldsymbol{\Omega}) \\ &\quad = \sum_{\ell=0}^{L} \frac{2\ell+1}{4\pi} \sum_{m=-\ell}^{\ell} \Big[\Sigma_{\mathrm{w},\ell}(\boldsymbol{r} + s\,\boldsymbol{\Omega})\, \phi^{m,(\kappa)}_\ell(\boldsymbol{r} + s\,\boldsymbol{\Omega}) \\ &\quad + Q^{\diamond m}_\ell(\boldsymbol{r} + s\,\boldsymbol{\Omega})\Big] R^m_\ell(\boldsymbol{\Omega}) \end{aligned} \tag{30}$$

$$\begin{aligned} &\boldsymbol{\Omega} \cdot \boldsymbol{\nabla} \delta\phi^{(\kappa+\frac{1}{2})}(\boldsymbol{r}, \boldsymbol{\Omega}) + \Sigma(\boldsymbol{r})\, \delta\phi^{(\kappa+\frac{1}{2})}(\boldsymbol{r}, \boldsymbol{\Omega}) \\ &\quad \frac{1}{4\pi}\Sigma_{\mathrm{w},0}(\boldsymbol{r})\, \delta\phi^{0,(\kappa+\frac{1}{2})}_0(\boldsymbol{r})\, R^m_\ell(\boldsymbol{\Omega}) \\ &\quad = \frac{1}{4\pi}\Sigma_{\mathrm{w},0}(\boldsymbol{r})\Big[\phi^{0,(\kappa+\frac{1}{2})}_0(\boldsymbol{r}) - \phi^{0,(\kappa)}_0(\boldsymbol{r})\Big] R^m_\ell(\boldsymbol{\Omega}) \end{aligned} \tag{31}$$

and

$$\phi^{(\kappa+1)}(\boldsymbol{r}, \boldsymbol{\Omega}) = \phi^{(\kappa+\frac{1}{2})}(\boldsymbol{r}, \boldsymbol{\Omega}) + \delta\phi^{(\kappa+\frac{1}{2})}(\boldsymbol{r}, \boldsymbol{\Omega}). \tag{32}$$

In the present work, Eq. (31) is a simplified transport equation with scattering isotropy and uniform (flat) sources. Moreover, we have choosen to solve this equation with the *Algebraic Collapsing* (AC) method, as presented in Ref. [6] and Sect. 3.10.3 of Ref. [1]. This choice is similar to the approach proposed by Alcouffe, consisting to replace Eq. (31)

by a form of the transport equation that is simpler to solve. In his work, Alcouffe proposed to replace Eq. (31) with a compatible *diffusion equation*, leading to the *diffusion synthetic acceleration* (DSA) scheme. A synthetic acceleration approach based on the AC method to solve Eq. (31) has been proposed and validated in the past, but only in cases where Eq. (30) is solved with the MOC with scattering isotropy and uniform (flat) sources.[8] The main contribution of this paper is to validate the use of a synthetic acceleration approach based on the AC method in cases with anisotropic scattering and linear sources.

IV. NUMERICAL RESULTS

The SC and LDC schemes with scattering anisotropy have been implemented in the DRAGON5 lattice code for 2D problems. These implementations were validated on a set of simple few-group benchmarks in fundamental mode condition (i. e., with reflective boundary conditions). We have performed convergence studies relative to three variants of the method of characteristics, namely the SC and LDC schemes, and with respect to increasing mesh refinement of the original Cartesian mesh. Note that our implementation of the method of characteristics is also compatible with unstructured meshes.

Statistics will be given for k_{eff} and absorption rate distribution accuracies. In all tables, N_{tot} is the total number of unknowns per energy group. Memory requirements are proportional to N_{tot}, as no matrices need to be stored. In all cases studied, a reference solution was established from a spatially converged calculation. Reference absorption rates $R^*_{\text{a},i}$ of assembly i were obtained with the following formula:

$$R^*_{\text{a},i} = \frac{1}{V_i} \int_{V_i} d^3r \, [\Sigma(\boldsymbol{r}) - \Sigma_{\text{s}}(\boldsymbol{r})] \, \phi(\boldsymbol{r}) \tag{33}$$

where $\Sigma_{\text{s}}(\boldsymbol{r})$ is the scattering cross section.

These reaction rates are then compared to data from less accurate calculations in order to obtain maximum $\epsilon_{\max}$ and average $\bar{\epsilon}$ errors.

1. The AIC assembly benchmark

We are investigating the application of the MOC in fundamental mode condition, focusing on specular boundary conditions obtained with the introduction of cyclic characteristics. We have constructed a four-group Cartesian mockup of a production eight-symmetry PWR assembly with five Silver-Indium-Cadmium (AIC) pins inserted. The corresponding geometry is depicted in Fig. 3. This benchmark retains many characteristics of a production assembly with more energy groups and with cylindrical pincells. The reactivity discrepancy between a P_0 and a P_1 scattering source is of the order of ≃2380 pcm. This discrepancy is reduced to ≃370 pcm if a transport correction is applied to the P_0 scattering source. Most lattice calculations are performed with a transport-corrected P_0 scattering source. In this case, an agreement with Monte Carlo better than 370 pcm is due to error compensation. This benchmark is therefore a good candidate for verifying both linear discontinuous and scattering anisotropy implementations of the neutrons sources in the MOC and for testing the effectiveness of the acceleration techniques.

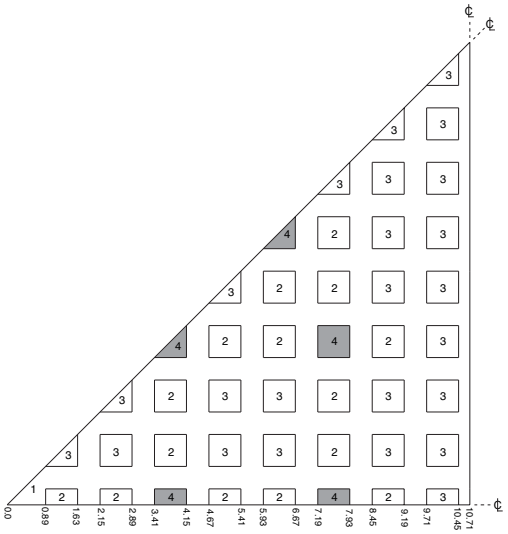

Fig. 3. Description of the AIC assembly benchmark. The dimensions are given in cm.

The MOC method with SC and schemes was implemented in DRAGON5 as described in the previous section. The `SALT:` module in DRAGON5 was used to generate a cyclic tracking with option "`TSPC 12 25.0`" set to select the number of planar angles and the number of tracks per cm. The cyclic tracks are computed on the eight-symmetry assembly, without unfolding the triangular domain. The reference solution is a DD2 approximation, with S_{18} level-symmetric quadrature and Submesh = 2 + 4.

Subm.	N_{tot}	k_{eff}	Δk_{eff} (pcm)	$\epsilon_{\max}$ (%)	$\bar{\epsilon}$ (%)	CPU (s)
1 + 1	513	0.908298	−654.1	2.35	0.54	2.4
2 + 4	3978	0.913206	−163.3	0.60	0.16	7.0
3 + 6	9009	0.914373	−46.6	0.24	0.06	10.4
4 + 8	15759	0.914882	4.3	0.20	0.06	17.4

Reference k_{eff} = 0.914839

TABLE I. MOC results for the AIC assembly benchmark with scattering anisotropy. Step characteristic (SC) scheme.

Subm.	N_{tot}	k_{eff}	Δk_{eff} (pcm)	$\epsilon_{\max}$ (%)	$\bar{\epsilon}$ (%)	CPU (s)
1 + 1	1539	0.914345	−47.3	0.87	0.11	6.8
2 + 4	11934	0.914397	−44.2	0.25	0.08	19.1

Reference k_{eff} = 0.914839

TABLE II. MOC results for the AIC assembly benchmark with scattering anisotropy. Linear discontinuous characteristic (LDC) scheme.

The implementation of ACA and GMRES(m) acceleration strategies were implemented in DRAGON5 as described in Sect. 3.10.3 of Ref. [1]. These strategies were applied

to the four-group AIC benchmark in order to determine their effectiveness in presence of scattering anisotropy and linear sources. The percent accuracy on the neutron flux in the fourth energy group is depicted in Figs. 5 and 6, corresponding to the step and linear discontinuous characteristic schemes, respectively. As expected, we observe a small decrease in effectiveness of the ACA method, if we compare Fig. 5 to Fig. 4 obtained for a case with scattering isotropy. The GMRES(m) effectiveness is not affected by scattering anisotropy and linear sources.

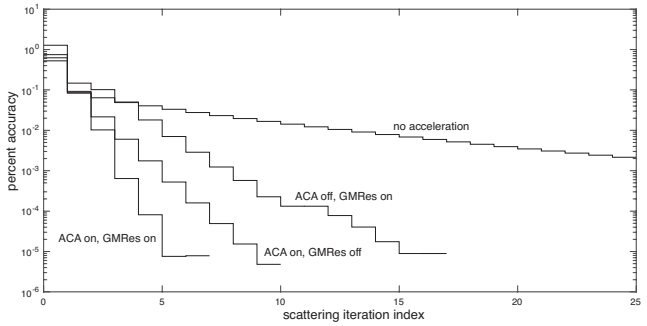

Fig. 4. Acceleration strategies for the MOC with SC scheme. Case with scattering isotropy.

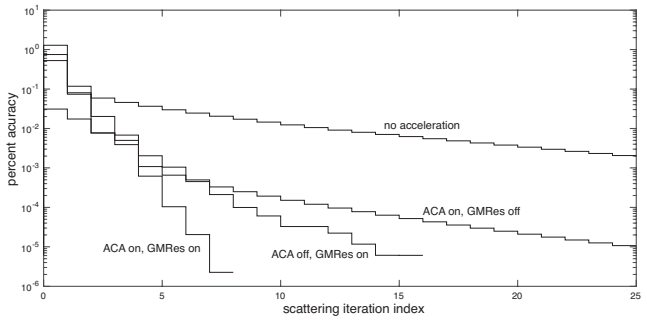

Fig. 5. Acceleration strategies for the MOC with SC scheme. Linear scattering anisotropy is present.

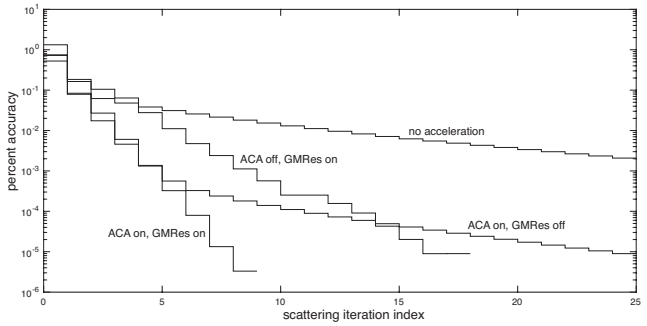

Fig. 6. Acceleration strategies for the MOC with LDC scheme. Linear scattering anisotropy is present.

V. CONCLUSIONS

The implementation of the MOC in DRAGON5 is based on low and high order differencing schemes along finite or cyclic characteristics. Two foundation papers were dedicated to implementations of the MOC related to finite and cyclic characteristics, respectively.[2, 3] This conference contribution completes the two foundation papers to cover issues related to acceleration of scattering iterations in presence of scattering anisotropy and linear discontinuous sources. We have shown that acceleration techniques such as ACA and GMRES(m) remain effective in these conditions, in spite of a small decrease in ACA effectiveness. The resulting MOC implementation is a therefore candidate for performing accurate lattice calculations in a code similar to DRAGON5.

REFERENCES

1. A. HÉBERT, *Applied Reactor Physics*, second edition, Presses Internationales Polytechnique, ISBN 978-2-553-01698-1, 396 p., Montréal, 2016. See the home page at `http://www.polymtl.ca/pub/`.
2. A. HÉBERT, "High-Order Diamond Differencing Along Finite Characteristics," *Nucl. Sci. Eng.* **169**, 81–97 (2011).
3. A. HÉBERT, "High Order Linear Discontinuous and Diamond Differencing Schemes along Cyclic Characteristics," *Nucl. Sci. Eng.* **184**, 591–603 (2016).
4. A. HÉBERT, "DRAGON5 and DONJON5, the contribution of École Polytechnique de Montréal to the SALOME platform," *Ann. nucl. Energy*, **87**, 12–20 (2016). See the home page at `http://www.polymtl.ca/merlin/`.
5. Y. SAAD and M. H. SCHULTZ, "GMRES: A Generalized Minimal RESidual Algorithm for Solving Nonsymmetric Linear Systems," *SIAM J. Sci. Stat. Comput.*, **7**, 856–869 (1986).
6. I. R. SUSLOV, "Solution of Transport Equation in 2- and 3-Dimensional Irregular Geometry by the Method of Characteristics," *Int. Conf. Math. Methods and Supercomputing in Nuclear Applications*, Karlsruhe, April 19–23, 1993.
7. R. E. ALCOUFFE, "Diffusion Synthetic Acceleration Methods for the Diamond Differenced Discrete Ordinates Equations," *Nucl. Sci. Eng.*, **64**, 344 (1977).
8. R. LE TELLIER and A. HÉBERT, "An improved Algebraic Collapsing Acceleration with General Boundary Conditions for the Characteristics Method," *Nucl. Sci. Eng.*, **156**, 121–138 (2007).